PAPER

Check for updates

Binuclear and tetranuclear Zn(II) complexes with thiosemicarbazones: synthesis, X-ray crystal structures, ATP-sensing, DNA-binding, phosphatase activity and theoretical calculations†

Piyali Adak,[a] Bipinbihari Ghosh,[a] Antonio Bauzá, [ID][b] Antonio Frontera, [ID] *[b] Steven R. Herron[c] and Shyamal Kumar Chattopadhyay [ID] *[a]

Two Zinc(II) complexes $[Zn_4(L^1)_4] \cdot 2H_2O$ (**1**) and $[Zn_2(L^2)_2] \cdot 2H_2O$ (**2**) of pyruvaldehydethiosemicarbazone ligands are reported. The complexes were characterized by elemental analysis, IR, NMR, UV-vis spectroscopy and by single-crystal X-ray crystallography. X-ray crystal structure determinations of the complexes show that though Zn : ligand stoichiometry is 1 : 1 in both the complexes, the molecular unit is tetranuclear for **1** and binuclear for **2**. Both the complexes show selective sensing of ATP at pH 7.4 (0.01 M HEPES) in CH_3CN-H_2O (9 : 1) medium in the presence of other anions like AcO^-, NO_3^-, F^-, Cl^-, $H_2PO_4^-$, HPO_4^{2-} and $P_2O_7^{2-}$. The UV-titration experiments of complexes **1** and **2** with ATP results in binding constants of $2.0(\pm0.07) \times 10^4$ M^{-1} and $7.1(\pm0.05) \times 10^3$ M^{-1} respectively. The calculated detection limits of 6.7 μM and 1.7 μM for **1** and **2** respectively suggest that the complexes are sensitive detectors of ATP. High selectivity of the complexes is confirmed by the addition of ATP in presence of an excess of other anions. DFT studies confirm that the ATP complexes are more favorable than those with the other inorganic phosphate anions, in agreement with the experimental results. Phosphatase like activity of both complexes is investigated spectrophotometrically using 4-nitrophenylphosphate (NPP) as a substrate, indicating the complexes possess significant phosphate ester hydrolytic efficiency. The kinetics for the hydrolysis of the substrate NPP was studied by the initial rate method at 25 °C. Michaelis–Menten derived kinetic parameters indicate that rate of hydrolysis of the P–O bond by complex **1** is much greater than that of complex **2**, the k_{cat} values being $212(\pm5)$ and $38(\pm2)$ h^{-1} respectively. The DNA binding studies of the complexes were investigated using electronic absorption spectroscopy and fluorescence quenching. The absorption spectral titrations of the complexes with DNA indicate that the CT-DNA binding affinity (K_b) of complex **1** $(2.10(\pm0.07) \times 10^6$ $M^{-1})$ is slightly greater than that of **2** $(1.11(\pm0.04) \times 10^6$ $M^{-1})$. From fluorescence spectra the apparent binding constant (K_{app}) values were calculated and they are found to be $5.41(\pm0.01) \times 10^5$ M^{-1} for **1** and $3.93(\pm0.02) \times 10^5$ M^{-1} for **2**. The molecular dynamics simulation demonstrates that the Zn(II) complex **1** is a good intercalator of DNA.

1. Introduction

The coordination chemistry of nitrogen–sulphur donor ligands towards transition metal ions[1,2] has attracted much attention and the interest arises in part from the fact that S-ligated transition metal complexes mimic the coordination environment of many biological systems. As a class of nitrogen–sulfur donor ligands, the synthesis of compounds incorporating thiosemicarbazones has attracted widespread attention of chemists as well as biologists, because of the interesting chemical, biological, structural and electronic properties of their metal complexes.[3–9] Again, Zn(II) ions play important roles in medicinal, chemical and biological events, and it is the second most abundant transition metal next to the iron ion in the body (human beings contain an average of 2–3 g of zinc), being vital in many cellular processes,[10] including gene expression,[11] apoptosis,[12] enzyme regulation[13] and neurotransmission.[14] It has been suggested that the anti-Alzheimer medicine clioquinol, a 8-hydroxyquinoline derivative, functions by way of

[a]Department of Chemistry, Indian Institute of Engineering Science and Technology, Shibpur, Howarh-711 103, India. E-mail: shch20@hotmail.com

[b]Department of Chemistry, University of the Balearic Islands, Carretera de Valldemossa km 7.5, 07122 Palma de Mallorca, IllesBalears, Spain

[c]Department of Chemistry, Utah Valley University, 800W University Pkwy, Orem UT 84058, USA

chelating Zn(II) along with Cu(II), the two metal ions which are critically associated with protein aggregation and degeneration processes in the brain.[15] Zinc complexes with N,S-donor sets are potential mimics of various zinc-containing metalloproteins.[16] The biological activity and the DNA-binding ability of zinc complexes have been the subject of a large number of studies.[17–19]

The design and synthesis of chemosensors for selective recognition and sensing of a particular anion is an area of immense importance.[20,21] Sensors that can detect and sense biologically important anions in aqueous environments and under physiological pH are of special significance owing to their potential applications in biological field.[22] Among various anions, recognition of phosphates, pyrophosphate, nucleotides, and nucleosides is important in this regard.[23,24] Among many phosphate anions, adenosine triphosphate (ATP) is most important as a molecular currency of intracellular energy transfer.[25]

Studies on the interaction of small molecules with DNA continue to attract considerable attention due to their importance in cancer therapy and molecular biology.[26–31] Over the last few decades, transition metal complexes that are capable of binding DNA under physiological conditions are of interest in the development of metal-based anticancer agents.[32–36] These complexes are used in DNA-footprinting studies, as sequence specific DNA binding agents, diagnostic agents in medicinal applications and for genomic research.[37–42]

On the other hand, over the years, much effort has been devoted to the development of metal complexes as models for metallo-enzymes catalyzing phosphate ester hydrolysis.[43] A number of zinc enzymes with multinuclear sites are known to be responsible for the hydrolysis of the phosphate esters.[44–53]

Herein we report the synthesis, characterization, and DNA binding property of two neutral tetranuclear and binuclear zinc(II) complexes which can be used to bind ATP in aqueous medium at physiological pH. These two zinc complexes effectively hydrolyses *p*-nitrophenylphosphate to *p*-nitrophenolate. The propensity of these complexes to bind to CT (calf-thymus) DNA has been investigated with UV-vis spectroscopic titration and their intrinsic binding constants, K_b, with CT-DNA have been determined. Competitive binding studies with ethidium bromide (EB), one of the most widely used intercalative agents and fluorescence probes for DNA structure, have been used in the study of the interaction of the complexes with CT-DNA in order to investigate a potential intercalative binding mode.

2. Experimental

2.1. Materials and methods

Pyruvic aldehyde, $Zn(CH_3COO)_2 \cdot 2H_2O$ were purchased from Aldrich. All other chemicals and solvents were of reagent grade and used as such. Solvents for spectroscopic and cyclic voltammetry were of HPLC grade obtained from Merck or Aldrich. Elemental analyses were performed on a PerkinElmer 2400 C, H, N analyzer. Infrared spectra were recorded as KBr pellets on a JASCO FT-IR-460 spectrophotometer. UV-vis spectra were recorded using a JASCO V-530 UV-vis spectrophotometer. ^1H

NMR spectra were recorded on a Bruker AVANCE DPX 300 MHz spectrometer using, $Si(CH_3)_4$ as internal standard. ESI-MS spectra of the samples were recorded on JEOL JMS 600 instrument.

2.2 Synthesis of ligand (HL)

The 4-(aryl)thiosemicarbazides were prepared from the corresponding aryl amines by the published procedure.[54] The thiosemicarbazones were prepared by refluxing (2 h) a methanolic solution of thiosemicarbazide with pyruvic aldehyde in 2 : 1 molar proportion.

Yield: ∼80–90%.

2.2.1   Ligand 1 (L^1H_2). Anal. calc. for: $C_{17}H_{18}N_6S_2$: C, 55.11; H, 4.90; N, 22.69. Found: C, 55.19; H, 4.97; N, 22.73%. ESI-MS, *m/z*: 371 [M + H]$^+$, 393 [M + Na]$^+$ (Fig. S1 in ESI†); ^1H NMR (DMSO-d$_6$) (δ ppm): 12.12 (1H, s), 10.78 (1H, s), 10.23 (1H, s), 10.04 (1H, s), 10.04 (1H, s), 7.55 (4H, m), 7.38 (4H, m), 7.22 (2H, m) 2.30 (3H, s) (Fig. S2 & S3 in ESI†); selected IR bands (cm^{-1}): 3296(ν_{NH}), 3152 (ν_{NH}), 1597 ($\nu_{C=N}$), 755 ($\nu_{C=S}$) (Fig. S13 in ESI†).

2.2.2   Ligand 2 (L^2H_2). Anal. calc. for $C_{19}H_{22}N_6S_2$: C, 57.26; H, 5.56; N, 21.09. Found: C, 57.18; H, 5.51; N, 21.05%. ESI-MS, *m/z*: 399 [M + H]$^+$ (Fig. S4 in ESI†); ^1H NMR (DMSO-d$_6$) (δ ppm): 12.06 (1H, s), 10.71 (1H, s), 10.14 (1H, s), 9.96 (1H, s), 7.84(1H, s), 7.38 (4H, m), 7.15 (4H, m), 2.31(3H, s), 2.28 (6H, s) (Fig. S5 & S6 in ESI†); selected IR bands (cm^{-1}): 3292 (ν_{NH}), 3156 (ν_{NH}), 1596 (sh, $\nu_{C=N}$), 730 ($\nu_{C=S}$) (Fig. S14 in ESI†).

2.3   Synthesis of the complexes

2.3.1   Synthesis of $[Zn_4(L^1)_4] \cdot 2H_2O$ (1). To a vigorously stirred methanolic suspension (15 ml) of the thiosemicarbazone ligand (L^1H_2) (370 mg, 1 mmol), Et$_3$N (202 mg, 2 mmol) was added. A solution of $Zn(CH_3COO)_2 \cdot 2H_2O$ (219 mg, 1 mmol) in methanol (10 ml) was added dropwise to the above solution. The solution turned orange. The mixture was stirred at room temperature for three hours and then filtered. The orange residue was washed with methanol and then dried over fused calcium chloride. The filtrate was allowed to evaporate slowly at room temperature when orange colored square shaped shiny crystals of complex $[Zn_4(L^1)_4] \cdot 2H_2O$ (1), suitable for X-ray diffraction studies, appeared after 4 days. Yield: 365 mg (84%). Anal. calc. for $C_{68}H_{68}N_{24}S_8O_2Zn_4$: C, 46.10; H, 3.87; N, 18.98. Found: C, 46.05; H, 3.80; N, 19.95%. ESI-MS, *m/z*: 432.91 [ZnL^1]$^+$ (Fig. S7 in ESI†); ^1H NMR (DMSO-d$_6$) (δ ppm): 9.67 (1H, s), 9.53 (1H, s), 7.86 (1H, s), 7.79 (4H, dd), 7.25 (4H, m), 6.94 (2H, dd), 2.25 (3H, s) (Fig. S8 & S9 in ESI†); electronic spectrum in DMF solution λ_{max}/nm (ε_{max}/M^{-1} cm^{-1}): 343(25 690), 460(39 847). Selected IR bands (cm^{-1}): 3290(ν_{NH}), 1600($\nu_{C=N}$), 1545($\nu_{C=N}$) (Fig. S13 in ESI†).

2.3.2   Synthesis of $[Zn_2(L^2)_2] \cdot 2DMF$ (2). This was synthesized following a similar procedure to that of **1**. Yield: 392 mg (85%). Anal. calc. for $C_{44}H_{54}N_{14}O_2S_4Zn_2$: C, 49.39; H, 5.09; N, 18.33. Found: C, 49.50; H, 4.98; N, 18.09 ESI-MS, *m/z*: 461.07 [ZnL^2]$^+$ (Fig. S10 in ESI†); ^1H NMR (DMSO-d$_6$): δ(ppm): 9.58 (1H, s), 9.43 (1H, s), 7.82 (1H, s), 7.66 (4H, m), 7.32 (4H, m), 2.27 (6H,s), 2.23 (3H, s) (Fig.s S11 & S12 in ESI†). Electronic spectrum in DMF solution λ_{max}/nm (ε_{max}/M^{-1} cm^{-1}): 342 (9814), 462

(15 964). Selected IR bands (cm^{-1}): 3151(ν_{NH}), 2952(ν_{NH}), 1589($\nu_{C=N}$) (Fig. S14 in ESI†). Single crystals suitable for X-ray structural analysis were obtained from the slow evaporation of the filtrate.

2.4 UV-vis titrations for anion sensing

Stock solutions of the Zn(II) complexes were prepared (1×10^{-5} M) in CH$_3$CN : H$_2$O (9 : 1, v/v) at pH 7.4 by using 20 mM HEPES buffer. The solution of the guest anion was prepared (2×10^{-4} M) in CH$_3$CN : H$_2$O (1 : 1, v/v) at pH 7.4 by using 20 mM HEPES buffer. The spectroscopic titrations were carried out by incremental addition of 0.02 ml (2×10^{-4} M) of anion solutions to the solution of the complexes **1** and **2** (1×10^{-5} M).

2.5 DNA-binding experiments

2.5.1 Absorption spectral studies. The binding experiments of the complexes (**1** and **2**) with CT-DNA were carried out in Tris–HCl buffer (50 mM, pH 7.4). A solution of CT-DNA in the buffer gave a ratio of UV absorbance at 260 and 280 nm of about 1.8–1.9 : 1, indicating that the DNA was sufficiently free from protein.[55] The DNA concentration per nucleotide and poly-nucleotide concentration were determined by absorption spectroscopy using the molar extinction coefficient (6600 M^{-1} cm^{-1}) at 260 nm.[56] The intrinsic binding constant K_b for the interaction of these metal (II) complexes with DNA has been calculated from the absorption spectral titration data. The intrinsic binding constant K_b was determined from,[57]

$$\frac{[\text{DNA}]}{\varepsilon_a - \varepsilon_f} = \frac{[\text{DNA}]}{\varepsilon_b - \varepsilon_f} + \frac{1}{K_b(\varepsilon_b - \varepsilon_f)}$$

The 'apparent' extinction coefficient (ε_a) was obtained by calculating A_{obs}/[Zn]. The symbols ε_f and ε_b correspond to the extinction coefficients of free (unbound) and the fully bound complexes. A plot of [DNA]/($\varepsilon_a - \varepsilon_f$) versus [DNA] will give a slope 1/($\varepsilon_b - \varepsilon_f$) and an intercept of 1/$K_b$ ($\varepsilon_b - \varepsilon_f$). Therefore K_b can be calculated from the ratio of the slope and intercept.[58]

2.5.2 Fluorescence spectral studies. The tetra and binuclear zinc(II) complexes do not exhibit luminescence, either in DMF or in the presence of calf thymus DNA. Therefore the binding of Zn(II) complexes to calf thymus DNA has been studied by competitive binding experiments. Ethidium bromide (EB) is well known to show fluorescence when bound to DNA due to intercalative binding with DNA.[59] The relative binding of the complexes with CT-DNA were studied using EB-bound CT-DNA solution in Tris–HCl buffer (pH 7.4). The fluorescence spectra were recorded at room temperature with excitation at 520 nm and emission at 610 nm. This experiment was carried out by titrating the complexes with EB-DNA solution containing 5×10^{-6} M EB and 5×10^{-6} M DNA.[60] The competitive binding of the zinc(II) complex to CT-DNA results in the displacement of the bound EB. This causes a decrease in the emission intensity due to fluorescence quenching of the free EB by the solvent molecules.[61–63] These spectroscopic features suggest that there exists an interaction between the zinc(II) complexes and DNA molecules.

2.6 Catalytic hydrolysis of 4-nitrophenyl phosphate

In order to study the phosphatase activity of the complexes, 10^{-4} M solutions of **1** and **2** in DMF were treated with 100 equiv. of 4-nitrophenyl phosphate in DMF–water(1 : 1) mixture under aerobic conditions at room temperature. The absorbance versus wavelength (wavelength scan) of these solutions was recorded at regular time intervals of 2 min in the wavelength range of 300–600 nm. To determine the dependence of the rate on the substrate concentration and various kinetic parameters, a 10^{-5} M solution of complex was treated with 10, 20, 30, 40, 50 and 100 equiv. of substrate. The reactions were followed spectrophotometrically by monitoring the increase in the absorbance at 427 nm (4-nitrophenolate band maximum) as a function of time (time scan).

The kinetics for the hydrolysis of the substrate NPP was determined by the initial rate method at 25 °C. The concentration of the substrate NPP was always kept at least 10 times larger than that of the complex and the increase of the 4-nitrophenol concentration was determined at 429 and 427 nm, respectively for the two complexes. For this purpose, 10^{-5} M solution of a complex was treated with the substrate solution having concentration ranging between 10-fold and 100-fold than that of the complex. Each kinetic experiment at a given substrate concentration was repeated thrice and average of the three values are taken. The dependence of the initial rate on the concentration of the substrates was monitored spectrophotometrically at the respective wavelengths. The initial rate method follows a first-order dependence on complex concentration since it showed saturation kinetics at higher substrate concentrations. For this reason, a treatment based on the Michaelis–Menten model was applied. The values of the Michaelis binding constant (K_M), maximum velocity (V_{max}) and rate constant for the dissociation of the substrate (i.e., turnover number, k_{cat}) were calculated for each complex by non-linear curve fitting using Michaelis–Menten equation:

$$V_0 = \frac{V_{max} + [S]}{K_M + [S]}$$

2.7 X-ray crystallography

Data for both the complexes were collected on a Burker APEX diffractometer at 293(2) K, using a graphite-monochromated Mo–Kα radiation. The data were solved by direct method and refined by full matrix least squares on F^2 using SHELX 97.[64] The non-hydrogen atoms were refined with anisotropic displacement parameters. All hydrogen atoms were placed at calculated positions and refined as riding atoms using isotropic displacement parameters. Corrections for Lorentz polarization effects and semiempirical absorptions were applied. A summary of the crystallographic data and the refinement details are summarized in Table 1. Important bond distances and bond angles are collected in Table 2.

2.8 Theoretical methods

2.8.1 DFT calculations. The geometries of the complexes used in this study were optimized with a density functional

Table 1 Crystal data and refinement details of complexes **1** and **2**

Formula	$C_{68}H_{64}N_{24}O_2S_8Zn_4$	$C_{44}H_{54}N_{14}O_2S_4Zn_2$
Formula weight	1767.48	1069.99
Crystal size(mm^3)	$0.22 \times 0.20 \times 0.10$	$0.26 \times 0.20 \times 0.12$
Temperature	293(2) K	273(2) K
Crystal system	Triclinic	Monoclinic
Space group	$P\bar{1}$	$P2_1/c$
a (Å)	10.454(3)	21.767(4)
b (Å)	10.621(4)	17.713(3)
c (Å)	19.648(6)	13.738(2)
α (°)	75.017(8)	90
β (°)	82.443(8)	103.454(4)
γ (°)	67.822(8)	90
d_{cal}	1.503	1.380
Z	1	4
μ(mm^{-1})	1.490	1.144
$F(000)$	902	2224
Total reflections	12 001	81 426
Unique reflections	3952	8614
Observed data [$I > 2\sigma(I)$]	2508	5368
R(int)	0.0737	0.0958
R_1, wR_2 [$I > 2\sigma(I)$]	0.0610, 0.1617	0.0752, 0.1343
R_1, wR_2 (all data)	0.1023, 0.1932	0.1391, 0.1675
Data/restraints/parameters	3952/0/480	8614/4/635
Goodness-of-fit (GOF) on F^2	1.011	1.137

theory (DFT) method by using the all-electron Dmol^3 program code of Accelrys, Inc.[65–67] The calculations were optimized at the UM06-L/DNP+ levels of theory, using the COSMO polarizable continuum model to mimic the water solvent effect. UM06-L is a local meta hybrid functional recommended for application in organometallic chemistry,[67] using double numerical with polarization and diffuse (DNP+) basis set and a global orbital cut off of 4.4 Å.[68]

2.8.2 Molecular dynamics calculation

A sequence of twelve base pairs of the oligonucleotide, d [GCGCGGAAGCGC]$_2$ like a model of calf thymus DNA was chosen and constructed in the double-helix B-DNA conformation by Discover Studio 4.0 of Accelrys inc. To create the intercalation pocket in the starting DNA structure, the torsion angles α–ξ of the sugar backbone were modified. The complex was intercalated in the major groove between 6th and 7th base pairs. We have used amber tools 12.0 (ref. 69) to create all input files to run the molecular dynamics simulations in Gromacs[70,71] software package. Molecular dynamics were performed using the amber14ipq Field to describe all parameters of the dodecamer. Partial charges for the Zn-complex were obtained using the restrained electrostatic fit (RESP) scheme. Electrostatic potentials were computed using the *ab initio* HF/6-31G(d) calculations using the Gaussian03 package.[72] All parameters of these molecules were taken from the general amber force field (GAFF) when we use the antechamber[73] software. Finally, all systems were neutralized with the addition of Na$^+$ ions and then were completed with a tetrahedral box of TIP3P waters to a depth of 1.0 nanometre on each side of the solutes.[74]

Preliminary energies minimizations were run with the steepest descent algorithm, during which the system

Table 2 Selected bond distances (Å) and angles (°) for **1** & **2**

1

Bond distances (Å)

Zn1–N3	2.115(8)	Zn2–N9	2.090(8)
Zn1–N4	2.124(8)	Zn2–N10	2.104(8)
Zn1–S2	2.330(3)	Zn2–S3	2.374(3)
Zn1–S1	2.347(3)	Zn2–S4	2.381(3)
Zn1–S3	2.545(3)	Zn2–S4	2.599(3)

Bond angles (°)

N3–Zn1–N4	73.8(4)	N9–Zn2–N10	74.6(3)
N3–Zn1–S2	146.4(2)	N9–Zn2–S3	80.8(3)
N4–Zn1–S2	80.5(3)	N10–Zn2–S3	148.8(2)
N3–Zn1–S1	80.3(3)	N9–Zn2–S4	154.4(3)
N4–Zn1–S1	152.4(3)	N10–Zn2–S4	80.6(2)
S2–Zn1–S1	118.73(10)	S3–Zn2–S4	119.97(10)
N3–Zn1–S3	103.5(2)	N9–Zn2–S4	93.8(2)
N4–Zn1–S3	94.3(2)	N10–Zn2–S4	99.5(2)
S2–Zn1–S3	99.58(10)	S3–Zn2–S4	101.02(9)
S1–Zn1–S3	100.97(10)	S4–Zn2–S4	96.18(8)

2

Bond distances (Å)

Zn1–N10	2.093(6)	Zn2–N3	2.094(5)
Zn1–N9	2.120(6)	Zn2–N4	2.113(5)
Zn1–S4	2.322(2)	Zn2–S1	2.4468(19)
Zn1–S3	2.447(2)	Zn2–S2	2.316(2)
Zn1–S1	2.454(2)	Zn2–S3	2.454(2)

Bond angles (°)

N10–Zn1–N9	74.4(2)	N3–Zn2–N4	74.9(2)
N10–Zn1–S4	81.65(18)	N3–Zn2–S2	80.67(16)
N9–Zn1–S4	148.91(17)	N4– Zn2– S2	147.36(17)
N10–Zn1–S3	147.50(18)	N3–Zn2–S1	147.40(16)
N9–Zn1–S3	78.24(17)	N4–Zn2–S1	78.40(16)
S4–Zn1–S3	115.98(7)	S2–Zn2–S1	114.84(7)
N10–Zn1–S1	105.95(17)	N3–Zn2–S3	107.01(17)
N9–Zn1–S1	100.75(18)	N4–Zn2–S3	100.86(16)
S4–Zn1–S1	104.71(8)	S2–Zn2–S3	106.80(8)
S3–Zn1–S1	95.99(6)	S1–Zn2–S3	96.00(6)

(oligonucleotide and the **1** complex) was restrained with a force constant of 1000 kJ mol^{-1} nm^{-2}, gradually relaxed to 100 kJ mol^{-1} nm^{-2}. Afterwards, a 100 ps equilibration step (NVT) was carried out using the modified Berendsen[75] thermostat to increase the temperature of the system at 300 K. A second 100 ps equilibration step was performed using the Parrinello–Rahman[76] pressure coupling model to equilibrate the pressure of the system at 1 atm. After the NVT and NPT steps, we run 500 ns molecular dynamic, enough to obtain well equilibrated MD trajectories of each system.

3. Results and discussion
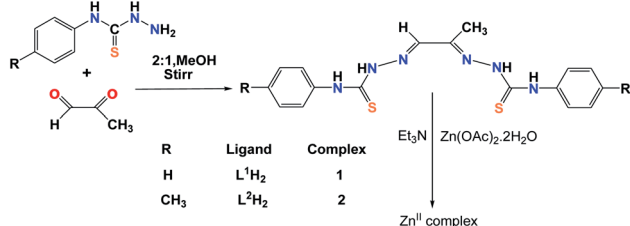
3.1 Synthesis of complexes

The Schiff base ligands used in this study were prepared following same method by stirring appropriate thiosemicarbazide derivatives with pyruvic aldehyde in 2 : 1 molar ratio. The Zn(II) complexes were obtained in moderately good

Paper

yield by reaction of the thiosemicarbazone Schiff bases with $Zn(OAc)_2 \cdot 2H_2O$ in presence of triethyl amine in 1 : 1 : 2 molar proportion in methanol at room temperature (Scheme 1). The ligands were characterized by elemental analysis, mass, IR and ^1H-NMR spectroscopy. For the ligand L^1H_2 tetranuclear Zn(II) complex was obtained, whereas for the ligand L^2H_2 binuclear Zn(II) complex was obtained. The solution stability of the complexes were ensured by measuring ESI-MS, NMR and UV-vis spectra of the complexes 8–10 hours after dissolution when the spectral data remain unchanged.

3.2 Description of X-ray crystal structure

X-ray crystal structure determination of complex **1** (Fig. 1 and 2) shows that though Zn : ligand stoichiometry is 1 : 1, the molecular unit is tetranuclear. The two central Zn(II) ions are bridged by two thiolato sulfur atoms in axial–equatorial mode, while each of the two terminal Zn(II) ions are connected to a central Zn(II) by a single thiolato bridge. Each of the four Zn(II) ions is in a square pyramidal N_2S_3-coordination environment, the equatorial position being occupied by one dideprotonated tetradentate ligand, and the axial position is occupied by a sulfur atom of a ligand attached to a neighbouring Zn(II) atom. Both the thiolato sulfur atoms belonging to the ligand attached to each of the central Zn(II) atoms participate in bridging while the sulfur atoms coordinated to the terminal Zn(II) atoms do not participate in bridging. The tetranuclear complex $[Zn_4(L^1)_4] \cdot 2H_2O$ (**1**) results from the pairing of two dinuclear units related by crystallographic centre of inversion, by two thiolato bridges. The distance between two central Zn(II) atom is 3.330(2) Å while the distance between the terminal and its adjacent Zn(II) atoms is 3·716(2) Å. The C–S bond distance lying between 1.734(10)–1.776(10) Å indicates the bis-thiosemicarbazone ligand binds through thiolate-like than thione-like. Sum of the different angles between the terminal metal centre and the donor atoms in its equatorial plane is 353.33(10)°, while that for the central metal center is 355.973(10)°, indicating the planarity of the tetradentate ligand. The coordination polyhedrons around Zn(II) centers may be described as axially elongated square pyramid with τ parameter being 0.09–0.10. The apical site of the coordination polyhedron is occupied by a bridging thiolato S-atom with Zn–S distance 2.545(3)–2.599(3) Å which is considerable longer than the Zn–S bond length (2.330(3)–2.381(3) Å) found in the basal plane.
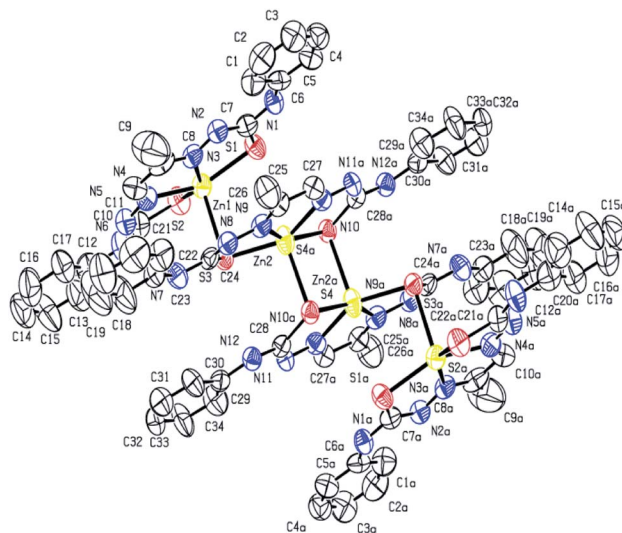

Fig. 1 ORTEP diagram (50% probability level) of $[Zn_4(L^1)_4] \cdot 2H_2O$ (**1**).

The structure of the binuclear complex is similar to the two doubly bridged central Zn(II) atoms of the tetranuclear complex with the terminal zinc centers being stripped off (Fig. 2). The Zn···Zn distance is 3.250(1) Å compared to 3.330(2) Å for the central Zn(II) atoms in the tetranuclear complex. The C–S bind distances lie in the range 1.739(8)–1.779(8) Å, with the bridging thiolate having slightly longer bond length. The Zn–N distances are almost identical in both the complexes, while the Zn–S distances are on an average slightly shorter in the binuclear complex.

3.3 Electronic spectra

The electronic spectra of the ligands and the complexes are depicted in Fig. 3. The free ligands show two bands, a strong sharp band at 350 nm and a very weak broad band at 460 nm. These bands are probably $\pi \rightarrow \pi^*$ (higher energy band) or $n \rightarrow \pi^*$ (lower energy band) in origin. In the complexes there is a strong transition at 460 nm. Extensive delocalization on deprotonation followed by complexation lowers the energy of
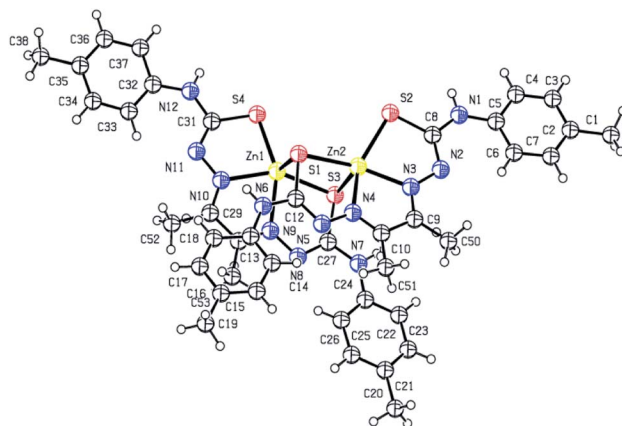

Scheme 1 Schematic representation of the template synthesis of the Zn(II) complexes.

Fig. 2 ORTEP diagram (50% probability level) of $[Zn_2(L^2)_2] \cdot 2H_2O$ (**2**).

the LUMO which is a π^*-orbital. The 460 nm band can have its origin in a new $\pi \rightarrow \pi^*$ transition or a LLCT transition from thiolate pπ to imine π^* orbital. The 350 nm band remains almost unaltered in complex **1** but in complex **2** it now appears as a shoulder.

3.4 ATP binding study

3.4.1 Absorption spectra study of zinc(ii) complexes to ATP. In order to study binding selectivity of complexes **1**and **2**, UV-vis titrations have been carried out at pH 7.4 in CH$_3$CN–H$_2$O (9 : 1) at a concentration of 10^{-5} M by adding salts of different anions. Fig. 4 and 5 display the notable changes in the UV-vis spectrum of **1** and **2** (10^{-5} M) on the addition of AcO$^-$, NO$_3^-$, F$^-$, Cl$^-$, H$_2$PO$_4^-$, HPO$_4^{2-}$, P$_2$O$_7^{2-}$ and ATP ions. Spectral changes were observed only when ATP is added to the solution. Moreover, the colour of the solutions **1** and **2** changed from yellow to colourless. However, no detectable spectral responses and colour changes were observed even after adding large amount of AcO$^-$, NO$_3^-$, F$^-$, Cl$^-$, H$_2$PO$_4^-$, HPO$_4^{2-}$ and P$_2$O$_7^{2-}$ ions. These results suggest that **1** and **2** can distinguish ATP from other anions.

To explore further about the applicability of **1** and **2** for ATP sensing, the UV-vis titrations were performed at pH 7.4 in CH$_3$CN–H$_2$O (9 : 1). The presence of ATP resulted in the significant increase of intensity of the absorbance band at 343 nm while the absorbance band at 450 nm decreases and the peak at 239 nm shifted to 260 nm with an increase in intensity for **1** (Fig. 4b). Upon the addition of ATP to **2**, the absorbance at 261 nm increases while the absorption at 450 nm gradually decreases. Moreover, a new absorption band appears at 349 nm, and its absorbance gradually increases with the addition of ATP (Fig. 5b). The competitive binding ability of ATP by the complexes in presence of three fold excess of other biologically important anions is shown in Fig. S16 in ESI.† It is clear from these two figures that both the complexes show high selectivity towards ATP.

The association constant (K_a) with ATP, as determined using a spectrophotometric titration method, for complexes **1** and **2** is found to be 2.0($\pm$0.07) $\times 10^4$ M^{-1} ($R^2 = 0.988$) and 7.1($\pm$0.05) $\times 10^3$ M^{-1} ($R^2 = 0.979$) respectively by using the Benesi–Hildebrand equation (Fig S17†). The calculated detection limits at 6.7 µM and 1.7 µM suggest that the complexes **1** and **2** are potentially very good sensors of ATP (Fig S18†).

Fig. 4 (a) UV-vis absorption changes of **1** upon addition of various anions at pH 7.4 (0.01 M HEPES) in CH$_3$CN–H$_2$O (9 : 1) medium. (b) UV-vis absorption titration spectra of **1** with ATP at pH 7.4 (0.01 M HEPES) in CH$_3$CN–H$_2$O (9 : 1) medium.

3.5 DNA binding studies

3.5.1 Absorption spectra. Electronic absorption spectroscopy is used for examining the binding modes of metal complexes with DNA. Hypochromic or bathochromic shift of the absorption band occurs due to strong stacking interaction between the aromatic chromophore of the complex and the adjacent base pairs of DNA. The interaction of the zinc(ii) complexes **1** and **2** in DMF solutions with CT-DNA was investigated by UV-vis titrations. Absorption titration experiments of the Zn(ii) complexes in Tris-buffer (pH 7.4) were performed using a fixed complex concentration to which increments of a DNA stock solution were added. The absorption band of complex **1** at 346 nm is red shifted and that at 460 nm is blue shifted with decrease of absorption intensity (Fig. 6a), while the absorption band of complex **2** at 277 nm and 463 nm both are blue shifted with decrease of absorption intensity (Fig. 6b). The binding constant values for **1** and **2** were calculated as 2.10 ($\pm$0.07) $\times 10^6$ ($R^2 = 0.986$) and 1.11($\pm$0.04) $\times 10^6$ ($R^2 = 0.99$), respectively (Fig. S18 and Table S1 in ESI†). The Gibb's free energy (ΔG) was calculated from eqn (1)

$$\Delta G = -RT \ln K \qquad (1)$$

where R is general gas constant (8.314 J K^{-1}mol^{-1}) and T is the temperature (298 K). The Gibb's free energy (ΔG) values for the **1**
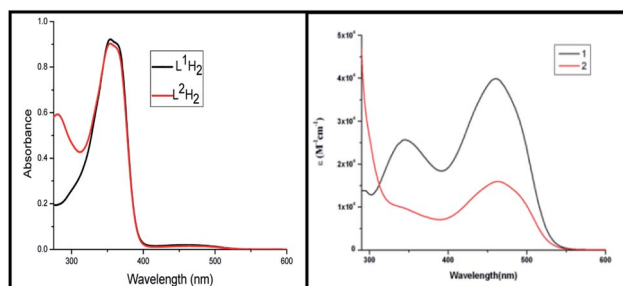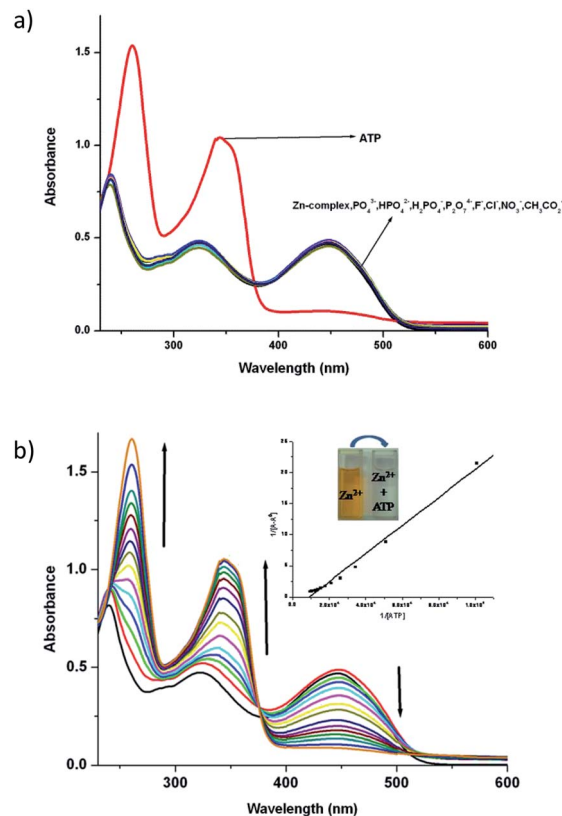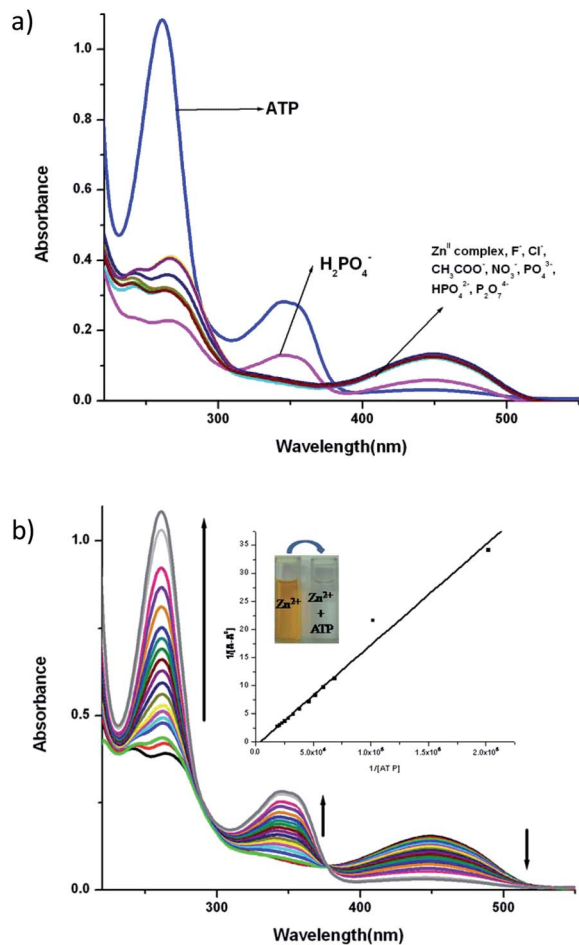

Fig. 3 UV-visible spectra of the ligands and the complexes in DMF at 298 K.

Fig. 5 (a) UV-vis absorption changes of **2** upon addition of various anions at pH 7.4 (0.01 M HEPES) in CH₃CN−H₂O (9 : 1) medium (b) UV-vis absorption titration spectra of **2** with ATP at pH 7.4 (0.01 M HEPES) in CH₃CN−H₂O (9 : 1)medium.
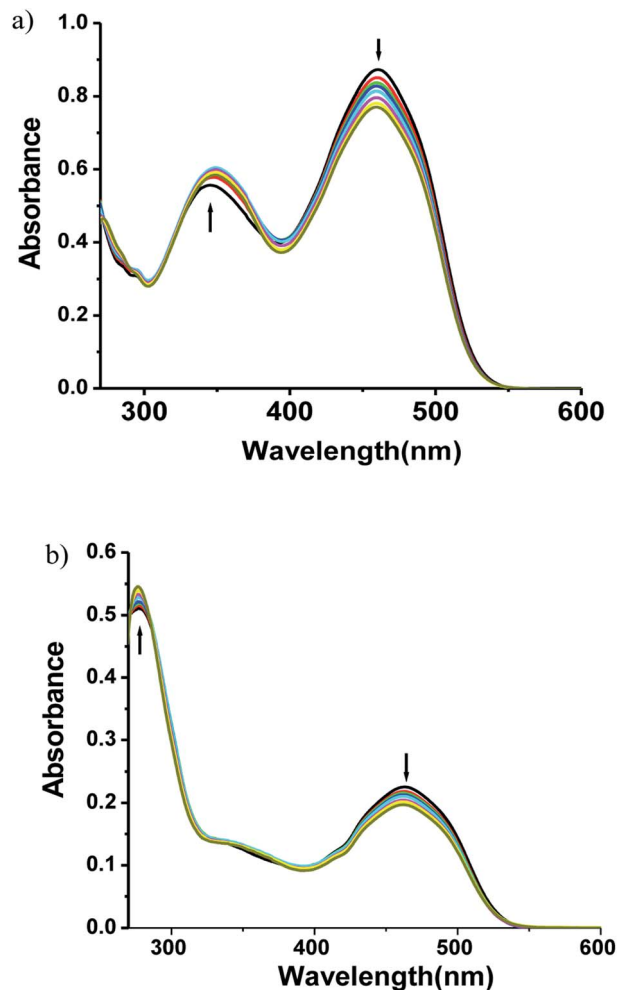

Fig. 6 Absorption spectra of (a) complex **1** (b) complex **2** (10^{-5} M) with increasing amounts of DNA at pH 7.4.

and **2** are -36.07 and -34.46 kJ mol^{-1} respectively. The moderately high negative values of ΔG indicate significant interactions of these compounds with DNA.

3.5.2 Fluorescence spectral studies. Complexes **1** and **2** show no fluorescence in DMF solutions both in presence as well as absence of DNA. So, to study the interaction between DNA and Zn(II) complexes we have chosen ethidium bromide(EB) as a fluorescence probe for DNA. Since the emission intensity of EB in buffer medium is low, but it is enhanced by its stacking interaction between adjacent DNA base pairs, so, the competitive DNA binding of the complexes has been studied by monitoring changes in the emission intensity of ethidium bromide (EB) bound to CT-DNA as a function of added complex concentration to get a proof for the binding of the complex to DNA *via* intercalation. When the complex was added to DNA pretreated with EB {[DNA]/[EB] = 1 : 1} at pH 7.4, the DNA-induced emission intensity of EB decreased (Fig. 7). Addition of a second DNA binding molecule would quench the EB emission by either accepting an excited state electron from EB or replacing the DNA-bound EB (if it binds to DNA more strongly than EB).

The emission spectra were monitored by keeping the excitation at 520 nm and the emission was monitored in the range of 540–690 nm. The emission was observed at 611 nm. The quenching constant K_{SV} was determined from the classical Stern–Volmer equation:[77]

$$\frac{I_0}{I} = 1 + K_{SV}[Q]$$

where I_0 and I are the fluorescence intensities in the absence and presence of complexes, respectively, K_{SV} is the linear Stern–Volmer quenching constant, [Q] is the concentration of the Zn(II) (quencher)complexes. The slope of the straight line gives the value of K_{SV} and the quenching constant value is $1.09(\pm0.007) \times 10^4$ and $5.87(\pm0.09) \times 10^3$ M^{-1} respectively (Table 3). The decrease in the fluorescence intensity thus proves the partial replacement of EB bound to DNA by complexes **1** and **2**. The apparent DNA binding constant (K_{app}) values of the complexes were obtained from the fluorescence spectral measurement. The K_{app} values were obtained from the equation: $K_{app} \times [\text{complex}]_{50} = K_{EB} \times [\text{EB}]$, where K_{app} is the apparent binding constant of the complex studied, [complex]$_{50}$
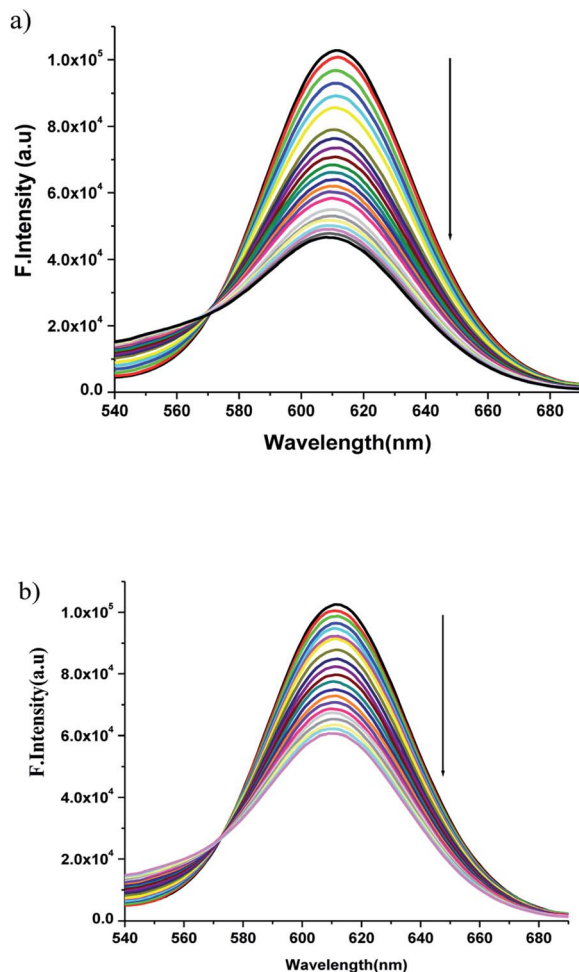
a)

b)

Fig. 7 Emission spectra of EB bound DNA with increasing amounts of the (a) complex **1** and (b) complex **2**. Arrow shows the intensity changes upon increasing the complex concentration.

a)

b)

Fig. 8 UV-vis spectral changes of complexes **1** (a), **2** (b) in DMF upon addition of 100 fold excess of NPP, observed at fixed intervals of time.

is the concentration of the complex at 50% quenching of DNA-bound ethidium bromide emission intensity, K_{EB} is the binding constant of ethidium bromide ($K_{EB} = 1 \cdot 0 \times 10^7$ M^{-1}), and [EB] is the concentration of ethidium bromide (5×10^{-6}).[78] The apparent binding constant (K_{app}) value was found to be $5.41(\pm 0.01) \times 10^5$ and $3.93(\pm 0.02) \times 10^5$ for complexes **1** and **2** respectively.

3.6 Kinetics of the hydrolysis of the phosphate ester PNPP

The phosphate ester hydrolysis ability of the complexes was evaluated using PNPP (4-nitrophenyl phosphate) as substrate.
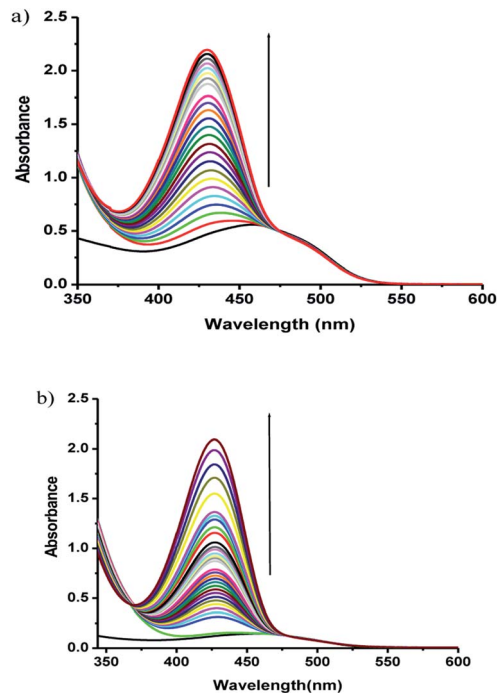
The reactions were carried out in DMF at 25 °C under aerobic conditions and were monitored by means of UV-vis spectroscopy. The time dependent spectral changes of the complexes **1** and **2** upon addition of NPP in DMF are shown in Fig. 8, which clearly demonstrate the gradual increment of the concentration of 4-nitro phenol ($\lambda_{max} = 400$ nm) with time (Fig. 8). These results suggest that both the complexes are active in catalyzing the hydrolysis of PNPP.

The enzyme kinetics data are listed in Table 4 and the kinetic plots are given in Fig. 9 and 10. The kinetic study indicated that complex **1** exhibits more than five times greater catalytic activity than complex **2**. Control experiments with PNPP only and PNPP mixed with zinc acetate solution shows negligible hydrolysis (Fig. S21†), confirming the efficacy of the complexes **1** and **2** as catalysts for the model phosphate ester hydrolysis reaction.

3.7 Theoretical calculations

We have divided the theoretical study into two different parts to analyze interesting aspects of the title compounds. First, we have analyzed the binding mechanism of the complex **1** to DNA by means of molecular dynamics simulations. Second, the

Table 3 DNA-binding data for the complexes

Complex	Electronic spectra			Fluorescence spectra		
	λ_{max} (nm)	Change in absorption	K_b(M^{-1})	λ_{max} (nm)	K_{SV}	K_{app}
1	460	Hypochromism	$2.10(\pm 0.07) \times 10^6$	611	$1.09(\pm 0.007) \times 10^4$	$5.41(\pm 0.01) \times 10^5$
2	463	Hypochromism	$1.11(\pm 0.04) \times 10^6$	611	$5.87(\pm 0.09) \times 10^3$	$3.93(\pm 0.02) \times 10^5$

Table 4 Kinetic parameters obtained from Michaelis–Menten plots for NPP hydrolysis by the zinc complexes

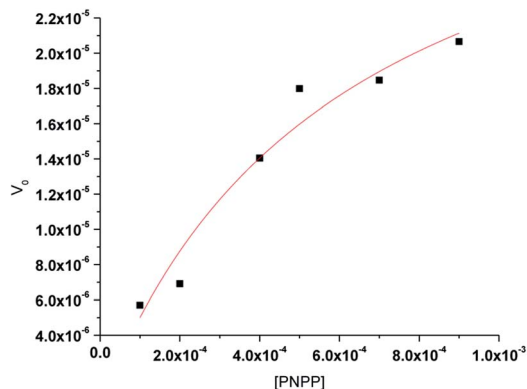| Complex	Wavelength (nm)	V_{max} (M min^{-1})	K_M (M)	R^2	k_{cat} (h^{-1})
1	429	$3.54(\pm0.67) \times 10^{-5}$	$6.08(\pm0.22) \times 10^{-4}$	0.947	212 ($\pm$5)
2	427	$6.25(\pm0.11) \times 10^{-6}$	$2.81(\pm0.13) \times 10^{-4}$	0.997	38($\pm$2)

Fig. 9 Michaelis–Menten plot for hydrolysis of PNPP by complex **1**.

binding geometries and energies of the ATP and related anions to complex **1** have been computed using DFT calculations in solution to rationalize its selectivity.

3.8 Molecular dynamics studies

Molecular dynamics (MD) simulations of the DNA oligonucle-otide has been used to investigate the intercalative binding of the complex **1** to DNA. The MD simulations of complex **1** like a model were conducted up to 500 ns in order to investigate if the metal complex stays in the intercalation site (Fig. 11). The complex was intercalated initially in the major grove. The nitrogenous bases sequence pair chosen around the complex were: G–C and A–T. After the first 75 ns of the simulation time, the complex finds the ideal orientation with respect to the nitrogenous bases. As we can see in the Fig. 12 one part of the complex intercalated perfectly within DNA, where there are
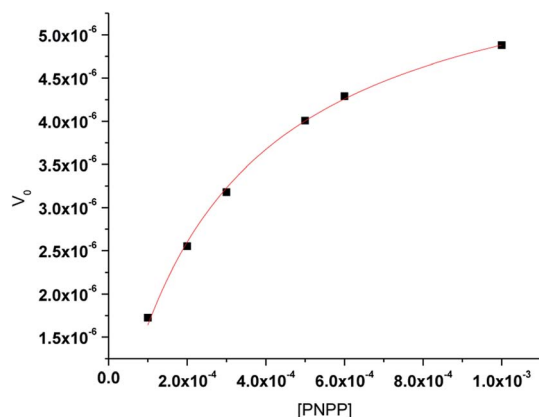
interactions with one phenyl and formaldehyde thio-semicarbazone groups with the nitrogenous bases of the pocket. On the other hand, the other phenyl is orientated outside the double helix. It is preserving this conformation for the remaining time of the simulation. In our case, the DNA oligonucleotide does not exhibit a significant mobility, espe-cially the central nitrogen bases.

An analysis of the statistical structures within the MD was carried out, finding three different bonding types between the Zn(II) complex **1** and the nucleobases: π–π stacking, metal–nucleobase bonding and hydrogen bonding interactions. Using the radial distribution function ($g(r)$), we calculate the complex–nitrogen base average distances throughout the simulation time. Fig. 12 and 13 represent these set of bonding between the complex and the bases around it.

The four nucleobases in the pocket present π–π stacking with some fraction of the complex intercalated. These interac-tions do not have the same intensity level. The cytosine base presents π–π stacking with a phenyl group with an average distance of 3.5 Å (yellow line in Fig. 13). This distance is in good agreement with the interplanar distance of 3.4–3.6 Å of benzene dimer. The remaining nucleobases (G, A, T) present similar average distances with the different thiosemicarbazone groups in the complex (blue arrows in Fig. 12 and grey, red and blue solid lines in Fig. 13, respectively). The guanine intensity in the radial distribution function is slightly higher than the intensity of the other nucleobases. This fact establishes that π–π stack-ing interactions are the most general in the pocket of the calf thymus DNA. Jointly, the guanine base presents two maximum intensity picks on a 2.6 Å and 2.9 Å average distances (dis-continues green and blue lines). This maximum in the function corresponds to the average distance of N3 group of guanine and O4′ of the sugar of the guanine. Interestingly, only this base

Fig. 10 Michaelis–Menten plot for hydrolysis of PNPP by complex **2**.
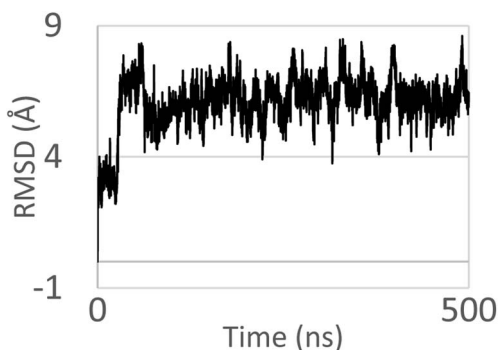
Fig. 11 RMSD obtained for the calf thymus DNA model and complex **1** up to 500 ns of MD simulations. RMSD of 6.070 ± 1.050 Å.
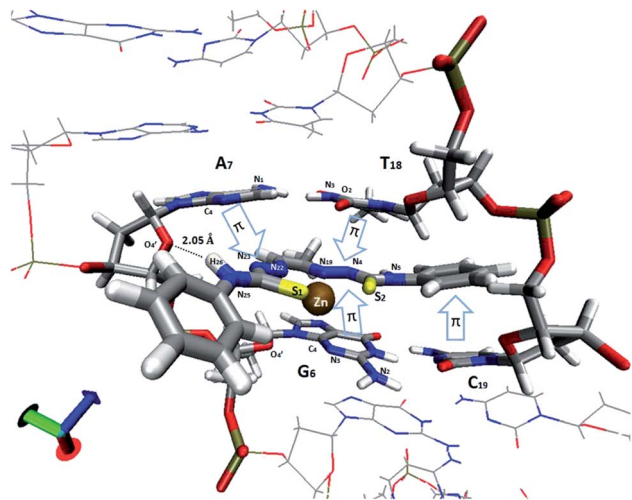
Fig. 12 View of the intercalation scheme of [Zn(L[1])] complex between G–C (6th and 7th residues, respectively) and A–T bases in the MD simulation. π–π stacking interactions are indicated with arrows.

shows bonding with the Zn in the complex. Finally, a strong and enduring hydrogen bond (2.0 Å average distance) in the MD simulation between the O4′ sugar of the adenine and H26 of the ligand complex is established.

The MD simulation demonstrates that the complex **1** is a good intercalator of DNA. The pocket design has been chosen in order to simulate the different bases within the DNA structure, finding an ideal orientation without needing a specific repetitive sequence in the oligonucleotide. Guanine base has a greater ability to interact with the complex through the Zn and π–π stacking and we assume that the presence of this nucleobase is necessary for the complex to interleave.

3.9 DFT study of the ATP binding to compound 1

We have studied the energetic and geometric features of complexes of compound **1** with ATP and also other phosphate anions (HPO_4^{2-} and $P_2O_7^{4-}$) for comparison purposes. The optimized complexes and binding energies are summarized in
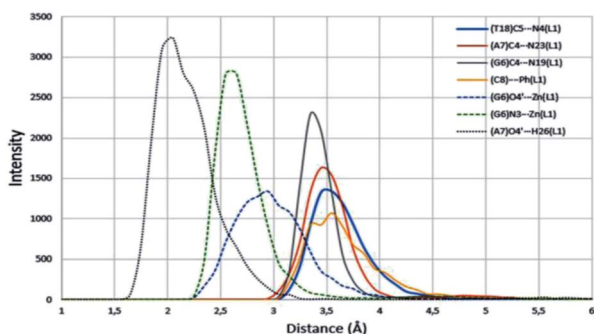

Fig. 13 Radial distribution functions of principal interactions between ZnL[1] complex and DNA. π–π stacking, metal bonding and hydrogen bonding are represented by solid, discontinues and points lines respectively. Average distances throughout the all simulation time.
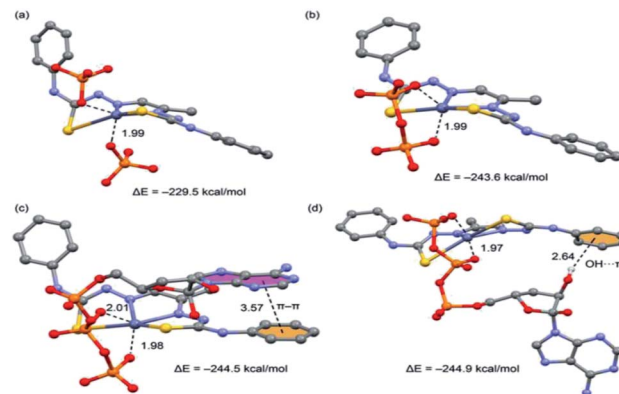

Fig. 14 (a–c) DFT optimized geometries of the complexes of **1** with several anions and ATP. (d) indicates the alternative mode of binding of ATP. Distances in Å. The binding energies are also indicated.

Fig. 14. It can be observed that the ATP complexes are more favorable than those with the other phosphorous inorganic anions, in agreement with the experimental results. The binding mode of the ATP is governed by two types of interactions, first, two strong Zn(II)···O interactions (coordination bonds) fix the geometry and explain the large binding energies obtained for the complexes. Moreover, the ATP presents additional interactions that explain its higher affinity to compound **1**. In fact, we have found two possible orientations for the ribose–adenine fragment that are almost isoenergetic and present different ancillary interaction. First, the adenine forms a stacking interaction with one phenyl ring of the organic ligand (Fig. 14(c)) and, second, one hydroxyl group of the sugar establishes an OH···π interaction with the organic ligand (Fig. 14(d)).

4. Conclusions

A tetranuclear and a binuclear complex of two tetradentate thiosemicarbazone ligands were synthesized, characterized and their sensing, DNA binding and catalytic properties were evaluated. The two zinc complexes can be used as ATP sensors at biological pH. The DNA binding experiment through UV-vis, fluorescence titrations suggest that the interaction between the complex and DNA is intercalative and the result suggest that complex **1** is more efficient than complex **2** to bind DNA at biological pH. The intercalation of compound **1** to DNA has been further demonstrated by means of molecular dynamics simulations. Both the complexes catalyze the hydrolysis of 4-nitrophenylphosphate to 4-nitrophenol.

Conflicts of interest

The authors declare no competing financial interest.

Acknowledgements

References

1 T. C. Harrop and P. K. Mascharak, *Acc. Chem. Res.*, 2004, **37**, 253–260.

2 T. Bal-Demirci, *Polyhedron*, 2008, **27**, 440–446.

3 M. J. M. Campbell, *Coord. Chem. Rev.*, 1975, **15**, 279–319.

4 S. Padhye and G. B. Kauffman, *Coord. Chem. Rev.*, 1985, **63**, 127–160.

5 D. X. West, S. B. Padhye and P. B. Sonowane, *Struct. Bonding*, 1991, **76**, 1–50.

6 D. X. West, A. E. Liberta, S. B. Chikate, P. B. Sonowane, A. S. Kumbhar and R. G. Yerande, *Coord. Chem. Rev.*, 1993, **123**, 49–71.

7 T. S. Lobana, R. Sharma, G. Bawa and S. Khanna, *Coord. Chem. Rev.*, 2009, **253**, 977–1055.

8 S. K. Chattopadhyay, in *Ruthenium: Properties, Production and Applications*, ed. D. B. Watson, Nova Publishers, 2011, pp. 293–310.

9 D. H. Petering, *Bioinorg. Chem.*, 1972, **1**, 255–271.

10 B. L. Vallee and K. H. Falchuk, *Physiol. Rev.*, 1993, **73**, 79–118.

11 K. H. Falchuk, *Biochem*, 1998, **188**, 41–48.

12 P. D. Zalewski, I. J. Forbes and W. H. Betts, *Biochem. J.*, 1993, **296**, 403–408.

13 W. Maret, C. Jacob and B. L. Vallee, *Proc. Natl. Acad. Sci. U.S.A.*, 1999, **96**, 1936–1940.

14 M. P. Cuajungco and G. J. Lees, *Neurobiol. Dis.*, 1997, **4**, 137169.

15 M. Di Vaira, C. Bazzicalupi, P. Orioli, L. Messori, B. Bruni and P. Zatta, *Inorg. Chem.*, 2004, **43**, 3795–3797.

16 A. Patra, S. Sarkar, R. Chakraborty, M. G. B. Drew and P. Chattopadhyay, *J. Coord. Chem.*, 2010, **63**, 1913–1920.

17 M. E. Anderson, A. G. M Barrett and B. M. Hoffman, *J. Inorg. Biochem.*, 2000, **80**, 257–260.

18 D. H. Tjahjono, S. Mima, T. Akutsu and N. Yoshioka, *J. Inorg. Biochem.*, 2001, **85**, 219–228.

19 T. Biver, F. Secco, M. R. Tine, M. Venturini, A. Bencini, A. Bianchi and C. Giorni, *J. Inorg. Biochem.*, 2004, **98**, 1531–1538.

20 (*a*) R. Martınez-Manez and F. Sancenon, *Chem. Rev.*, 2003, **103**, 4419–4476; (*b*) C. Suksai and T. Tuntulani, *Chem. Soc. Rev.*, 2003, **32**, 192–202; (*c*) P. D. Beer and P. A. Gale, *Angew. Chem., Int. Ed.*, 2001, **40**, 486–516; (*d*) A. P. de Silva, H. Q. N. Gunaratne, T. Gunnlaugson, A. J. M. Huxley, C. P. McCoy, J. T. Rademacher and T. E. Rice, *Chem. Rev.*, 1997, **97**, 1515–1566; (*e*) P. A. Gale, *Acc. Chem. Res.*, 2006, **39**, 465–475.

21 (*a*) D. A. Jose, D. K. Kumar, B. Ganguly and A. Das, *Org. Lett.*, 2004, **6**, 3445–3448; (*b*) D. A. Jose, D. K. Kumar, B. Ganguly and A. Das, *Tetrahedron Lett.*, 2005, **46**, 5343–5346.

22 (*a*) B. S. Khakh and R. A. North, *Nature*, 2006, **442**, 527–532; (*b*) N. StojanovicMilan, *US Pat.* Appl. Publ., US 2006172320, 2006; (*c*) Z. Kejík, K. Záruba, D. Michalík, J. Sebek, J. Dian, S. Pataridis, K. Volka and V. Král, *Chem. Commun.*, 2006, 1533–1535; (*d*) A. Jaime, R. Belin and D. Astruc, *Angew. Chem., Int. Ed.*, 2006, **45**, 132–136; (*e*) D. H. Lee, S. Y. Kim and J.-I. Hong, *Angew. Chem., Int. Ed.*, 2004, **43**, 4777–4780;

(*f*) M. S. Han and D. H. Kim, *Angew. Chem., Int. Ed.*, 2002, **41**, 3809–3811; (*g*) A. Ojida, M. Yoshifumi, W. Jirarut, T. Shun-ichi, K. Sada and I. Hamachi, *Chem. - Asian J.*, 2006, **1**, 555–563.

23 (*a*) A. K. H. Hirsch, F. R. Fischer and F. Diederich, *Angew. Chem., Int. Ed.*, 2007, **46**, 338–352; (*b*) Y. J. Jang, E. J. Jun, Y. J. Lee, Y. S. Kim, J. S. Kimand and J. Yoon, *J. Org. Chem.*, 2005, **70**, 9603–9606; (*c*) H. K. Cho, D. H. Lee and J.-I. Hong, *Chem. Commun.*, 2005, 1690–1692; (*d*) D. H. Lee, J. H. Im, S. U. Son, Y. K. Chung and J.-I. Hong, *J. Am. Chem. Soc.*, 2003, **125**, 7752–7753; (*e*) S. Mizukami, T. Nagano, Y. Urano, A. Odani and K. Kikuchi, *J. Am. Chem. Soc.*, 2002, **124**, 3920–3925; (*f*) L. Fabbrizzi, N. Marcotte, F. Stomeo and A. Taglietti, *Angew. Chem., Int. Ed.*, 2002, **41**, 3811–3814.

24 (*a*) J. K. Kwon, N. J. Singh, H. N. Kim, S. K. Kim, K. S. Kim and J. Yoon, *J. Am. Chem. Soc.*, 2004, **126**, 8892–8893; (*b*) A. Ojida, Y. Mito-oka, K. Sada and I. Hamachi, *J. Am. Chem. Soc.*, 2004, **126**, 2454–2463.

25 P. Ritter, *Biochemistry*, 1999, **36**, 1996.

26 L. R. Kelland, *Eur. J. Cancer*, 2005, **41**, 971–979.

27 C. Metcalfe and J. A. Thomas, *Chem. Soc. Rev.*, 2003, **32**, 215–224.

28 A. Ray, G. M. Rosair, R. Kadam and S. Mitra, *Polyhedron*, 2009, **28**, 796–806.

29 K. H. Thompson and C. Orvig, *Dalton Trans.*, 2006, 761–764.

30 Y. Chen, Y. J. Liu, Q. Li and K. Z. Wang, *J. Inorg. Biochem.*, 2009, **103**, 1395–1404.

31 F. Li, W. Chen, C. Tang and S. Zhang, *Talanta*, 2008, **77**, 1–8.

32 F. A. Beckford, J. Thessing, A. Stott, A. A. Holder, O. G. Poluektov, L. Li and N. P. Seeram, *Inorg. Chem. Commun.*, 2012, **15**, 225–229.

33 J. G. Liu, B. H. Ye, H. Li, Q. X. Zhen, L. N. Ji and Y. H. Fu, *J. Inorg. Biochem.*, 1999, **76**, 265–271.

34 B. Cvek, V. Milacic, J. Taraba and Q. P. Dou, *J. Med. Chem.*, 2008, **51**, 6256–6258.

35 V. Milacic, D. Chen, L. Giovagnini, A. Diez, D. Fregona and Q. P. Dou, *Toxicol. Appl. Pharmacol.*, 2008, **231**, 24–33.

36 N. Farrell, *Compr. Coord. Chem. II*, 2003, **9**, 809–840.

37 M. D. Kuwabara, C. Yoon, T. E. Goyne, T. Thederahn and D. S. Sigman, *Biochemistry*, 1986, **25**, 7401–7408.

38 N. Raman, S. Sobha and A. Thamaraichelvan, *Spectrochim. Acta, Part A*, 2011, **78**, 888–898.

39 F. R. Keene, J. A. Smith and J. G. Collins, *Coord. Chem. Rev.*, 2009, **253**, 2021–2035.

40 B. H. Geierstanger, M. Mrksich, P. B. Dervan and D. E. Wemmer, *Science*, 1994, **266**, 646–650.

41 P. Krishnamoorthy, P. Sathyadevi, A. H. Cowley, R. R. Butorac and N. Dharmaraj, *Eur. J. Med. Chem.*, 2011, **46**, 3376–3387.

42 R. C. Sharma and V. K. Varshney, *J. Inorg. Biochem.*, 1991, **41**, 299–304.

43 R. Krämer, *Coord. Chem. Rev.*, 1999, **182**, 243–261.

44 (*a*) D. Gani and J. Wilkie, *Chem. Soc. Rev.*, 1995, 55–63; (*b*) W. N. Lipscomb and N. Strater, *Chem. Rev.*, 1996, **96**, 2375–2484; (*c*) D. E. Wilcox, *Chem. Rev.*, 1996, **96**, 2435–2458.
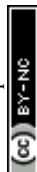
45 H. Steinhagen and G. Helmchen, *Angew. Chem., Int. Ed. Engl.*, 1996, **35**, 2339–2342.

46 N. Strater, W. N. Lipscomb, T. Klabunde and B. Kerbs, *Angew. Chem., Int. Ed. Engl.*, 1996, **35**, 2024–2055.

47 P. Gettins and J. E. Coleman, *J. Biol. Chem.*, 1984, **259**, 4991–4997.

48 L. Ma, T. T. Tibbitts and E. R. Kantrowitz, *Protein Sci.*, 1995, **4**, 1498–1506.

49 F. Hollfelder and D. Herschlag, *Biochemistry*, 1995, **34**, 1225512264.

50 J. E. Murphy, T. T. Tibbitts and E. RKantrovitz, *J. Mol. Biol.*, 1995, **253**, 604–617.

51 E. Hough, L. K. Hansen, B. Birkens, K. Jynge, S. Hansen, A. Hardvik, C. Little, E. Dodson and Z. Derewenda, *Nature*, 1989, **338**, 357.

52 E. E. Kim and H. W. Wyckoff, *J. Mol. Biol.*, 1991, **218**, 449–464.

53 J. E. Coleman, *Annu. Rev. Biophys. Biomol. Struct.*, 1992, **21**, 441–483.

54 A. B. Sen and S. K. Sengupta, *J. Indian Chem. Soc.*, 1962, **39**, 628.

55 S. Satyanarayana, J. C. Dabrowiak and J. B. Chaires, *Biochemistry*, 1993, **32**, 2573–2584.

56 J. K. Barton, J. M. Goldberg, C. V. Kumar and N. J. Turro, *J. Am. Chem. Soc.*, 1986, **108**, 2081–2088.

57 A. M. Pyle, J. P. Rehmann, R. Meshoyrer, C. V. Kumar, N. J. Turro and J. K. Barton, *J. Am. Chem. Soc.*, 1989, **111**, 3051–3058.

58 P. R. Reddy, A. Shilpa, N. Raju and P. Raghavaiah, *J. Inorg. Biochem.*, 2011, **105**, 1603–1612.

59 A. K. Patra, S. Roy and A. R. Chakravarty, *Inorg. Chim. Acta*, 2009, **362**, 1591–1599.

60 G. J. Chen, X. Qiao, P. Q. Qiao, G. J. Xu, J. Y. Xu, J. L. Tian, W. Gu, X. Liu and S. P. Yan, *J. Inorg. Biochem.*, 2011, **105**, 119–126.

61 C. L. Liu, J. Y. Zhou and H. B. Xu, *J. Inorg. Biochem.*, 1998, **71**, 1–6.

62 S. Mahadevan and M. Palaniandavar, *Inorg. Chem.*, 1998, **37**, 3927–3934.

63 X. M. Xu, J. H. Yao, Z. W. Mao, K. B. Yu and L. N. Ji, *Inorg. Chem. Commun.*, 2004, **7**, 803–805.

64 G. M. Sheldrick, *Acta Crystallogr., Sect. A: Found. Crystallogr.*, 2008, **64**, 112–122.

65 B. Delley, *J. Chem. Phys.*, 2000, **113**, 7756.

66 B. Delley, *J. Phys. Chem.*, 1996, **100**, 6107–6110.

67 Y. Zhao and D. G. Truhlar, *J. Chem. Phys.*, 2006, **125**, 194101.

68 B. Delley, *J. Chem. Phys.*, 1990, **92**, 508.

69 D. A. Case, T. A. Darden, T. E. Cheatham III, C. L. Simmerling, J. Wang, R. E. Duke, R. Luo, R. C. Walker, W. Zhang, K. M. Merz, B. Roberts, S. Hayik, A. Roitberg, G. Seabra, J. Swails, A. W. Götz, I. Kolossváry, K. F. Wong, F. Paesani, J. Vanicek, R. M. Wolf, J. Liu, X. Wu, S. R. Brozell, T. Steinbrecher, H. Gohlke, Q. Cai, X. Ye, J. Wang, M. J. Hsieh, G. Cui, D. R. Roe, D. H. Mathews, M. G. Seetin, R. Salomon-Ferrer, C. Sagui, V. Babin, T. Luchko, S. Gusarov, A. Kovalenko and P. A. Kollman , *AMBER 12*, University of California, San Francisco, 2012.

70 D. van der Spoel, E. Lindahl, B. Hess, G. Groenhof, A. E. Mark and H. J. C. Berendsen, *J. Comput. Chem.*, 2005, **26**(16), 1701–1718.

71 B. Hess, C. Kutzner, D. van der Spoel and E. Lindahl, *J. Chem. Theor. Comput.*, 2008, **4**(3), 435–447.

72 M. J. Frisch, G. W. Trucks, H. B. Schlegel, G. E. Scuseria, M. A. Robb, J. R. Cheeseman Jr, J. A. Montgomery, T. Vreven, K. N. Kudin, J. C. Burant, J. M. Millam, S. S. Iyengar, J. Tomasi, V. Barone, B. Mennucci, M. Cossi, G. Scalmani, N. Rega, G. A. Petersson, H. Nakatsuji, M. Hada, M. Ehara, K. Toyota, R. Fukuda, J. Hasegawa, M. Ishida, T. Nakajima, Y. Honda, O. Kitao, H. Nakai, M. Klene, X. Li, J. E. Knox, H. P. Hratchian, J. B. Cross, V. Bakken, C. Adamo, J. Jaramillo, R. Gomperts, R. E. Stratmann, O. Yazyev, A. J. Austin, R. Cammi, C. Pomelli, J. W. Ochterski, P. Y. Ayala, K. Morokuma, G. A. Voth, P. Salvador, J. J. Dannenberg, V. G. Zakrzewski, S. Dapprich, A. D. Daniels, M. C. Strain, O. Farkas, D. K. Malick, A. D. Rabuck, K. Raghavachari, J. B. Foresman, J. V. Ortiz, Q. Cui, A. G. Baboul, S. Clifford, J. Cioslowski, B. B. Stefanov, G. Liu, A. Liashenko, P. Piskorz, I. Komaromi, R. L. Martin, D. J. Fox, T. Keith, M. A. Al-Laham, C. Y. Peng, A. Nanayakkara, M. Challacombe, P. M. W. Gill, B. Johnson, W. Chen, M. W. Wong, C. Gonzalez, and J. Pople, A, *Gaussian 03, Revision C.02*, Gaussian, Inc., Wallingford CT, 2004.

73 J. Wang, W. Wang, P. A. Kollman and D. A. Case, *J. Mol. Graphics Modell.*, 2006, **25**(2), 247–260.

74 W. L. Jorgensen, J. Chandrasekhar, J. D. Madura, R. W. Impey and M. L. Klein, *J. Chem. Phys.*, 1983, **79**(2), 926.

75 H. J. C. Berendsen, J. P. M. Postma, W. F. Vangunsteren, A. Dinola and J. R. Haak, *J. Chem. Phys.*, 1984, **81**(8), 3684.

76 M. Parrinello and A. Rahman, *J. Appl. Phys.*, 1981, **52**(12), 7182.

77 P. X. Xi, Z. H. Xu, X. H. Liu, F. J. Chen and Z. Z. Zeng, *Chem. Pharm. Bull.*, 2008, **56**, 541–546.

78 M. Lee, A. L. Rhodes, M. D. Wyatt, S. Forrow and J. A. Hartley, *Biochemistry*, 1993, **32**, 4237–4245.